What causes the excessive response of clear-sky greenhouse effect to El Niño warming in Community Atmosphere Models?

Tao Zhang and De-Zheng Sun

Cooperative Institute for Research in Environmental Sciences

University of Colorado/NOAA Earth System Research Laboratory

Physical Sciences Division

Boulder, Colorado

E-mail: tao.zhang@noaa.gov

Accepted on November 5, 2007

(Submitted to *J. Geophys. Res*.)

Abstract

To diagnose the causes of an excessive response of the clear-sky greenhouse effect to El Niño warming in the Community Atmosphere Models (CAMs), the response of both water vapor and temperature to El Niño warming in the models is examined as a function of height. The percentage response of water vapor to El Niño warming in the models is considerably stronger than the response in the NCEP reanalysis in the middle and upper troposphere (700mb-300mb). The maximum discrepancy with NCEP data at 500 mb reaches 18%/K in CAM3. The discrepancy in the temperature response between the models and NCEP data at all tropospheric levels is within 0.3 K/K, with the maximum discrepancy occurring in the immediate neighborhood of 600 mb. The comparison between the models and ERA-40 reanalysis leads to the similar results.

Employing a radiative model, we have calculated the contributions of the excessive water vapor response in the middle and upper troposphere and the contributions from the differences in the lapse rate response to the discrepancies seen in the clear-sky greenhouse effect. The results confirm that the main cause of the excessive response of the clear-sky greenhouse effect is an excessive response of water vapor in the middle and upper troposphere. The excessive response of upper tropospheric water vapor is found to be accompanied with an excessive response in the upper cloud cover and vertical motion. Biases in both phases of ENSO contribute to these excessive responses to ENSO.

1. Introduction

Water vapor is the major contributor to the greenhouse effect of the earth's atmosphere (Kiehl and Trenberth 1997). Its contribution is usually measured by the so-called clear-sky greenhouse effect (Raval and Ramanathan 1989)—the difference between the longwave emission by the surface and the outgoing longwave radiation at the top of atmosphere in cloud-free situation. The response of the clear-sky greenhouse effect to a change in SST has been conveniently referred to as the water vapor feedback, although it also includes the feedback from the lapse rate (Sun and Lindzen 1993; Inamdar and Ramanathan 1994; Held and Soden 2000). Water vapor feedback is potentially the strongest positive feedback that amplifies human-induced global warming (Houghton et al. 2001). As we increasingly rely on climate models to assess and predict climate change, we need to critically assess the accuracy of water vapor feedback in climate models (Stocker et al. 2001, Sun et al. 2001, Sun et al. 2006, Sun et al. 2007).

The response of water vapor to El Niño warming stands as a useful test bed to isolate and fix potential errors in our simulations of water vapor feedback. This is because the signal is strong, planetary in spatial scale, and has a time scale on which we have good observations. Earlier studies have stressed that El Niño warming is not a good surrogate for global warming because the latter may have a different spatial pattern of warming (Sun and Held 1996 and others). This argument has given back some ground recently as more and more climate models predict El Niño-like warming in response to increases in

the greenhouse gases (Meehl and Washington 1996; Timmerman et al. 1999; Cai and Whetton 2000; Boer et al. 2004). Exactly how the climate system responds to anthropogenic forcing may take some time to answer. Fortunately, the need to document carefully and understand the discrepancies between model simulated response of the greenhouse effect of water vapor and that indicated in available observations does not depend much on the answer to this question.

In an earlier study of water vapor feedback in the CCM3 (CAM1), Sun et al. (2003) found that the response of the clear-sky greenhouse effect to El Niño warming in the model is considerably larger than that indicated in the ERBE observations. In an extended study by Sun et al. (2006), they found that three recent versions of the Community Atmosphere Model (CAM) continue to overestimate the response of clear-sky greenhouse effect to El Niño warming.

The clear-sky greenhouse effect depends on the water vapor as well as on the lapse rate (Sun and Lindzen 1993; Held and Soden 2000). Therefore there are two possible causes of the excessive response in the clear-sky greenhouse effect. One is that the response of the water vapor concentration in the troposphere is too strong in the model. The other possibility is that the lapse rate response in the models is not the same as in the observations. We would like to know the relative contributions from these two processes to the excessive response in the clear-sky greenhouse effect noted in the models. Therefore we examine in this paper the vertical structure of both the water vapor and

temperature response to El Niño warming, and we will quantify the contributions from these two factors to the discrepancies seen in the response of the clear-sky greenhouse effect.

2. Methodology, data and model

The clear-sky greenhouse effect is defined as the difference between the surface emission and the clear-sky outgoing longwave radiation (OLR) at the top of the atmosphere (see equation (1) of Zhang and Sun (2006)). We employ the same regression analysis of Zhang and Sun (2006) in this study. Note that the regression coefficients are obtained by using interannual variations of greenhouse effect over ocean regions only. As we attempt to understand the discrepancy in the clear-sky greenhouse effect between those in the models and that from ERBE (Barkstrom 1984), we again focus on the ERBE period (February 1985 − April 1989).

The clear-sky OLR from the ERBE S-4 data product archived in NCAR Climate and Global Dynamics Division (CGD) is used to calculate the clear-sky greenhouse effect from ERBE observations (see http://www.cgd.ucar.edu/cas/catalog/satellite/erbe/). We adopt the modified monthly mean data in this study that have been reprocessed to accommodate the discontinuity that occurred with the loss of NOAA-9 in January 1987. To examine the vertical structure of the water vapor and temperature response, we also employ the clear-sky OLR data from the National Centers for Environmental

Prediction-National Center for Atmospheric Research (NCEP-NCAR) reanalysis (Kalnay et al. 1996) to obtain clear-sky greenhouse effect from NCEP reanalysis.

Observations of cloud cover are obtained from the International Satellite Cloud Climate Project (ISCCP) data (Rossow et al., 1996; Rossow and Schiffer, 1999). Note that in obtaining the middle and low cloud level, ISCCP cloud cover has been adjusted for cloud layering assuming a random cloud overlap. The detailed discussion of ISCCP cloud overlap is given by Sun et al. (2003). The specific humidity, air temperature, and vertical velocity data from NCEP reanalysis are mainly used to examine the model simulations in the present study. For comparison, we also use the European Centre for Medium-Range Weather Forecasts (ECMWF) reanalyses ERA-40 (Uppala et al., 2005) to evaluate the response of water vapor and temperature from the models. The observed SSTs are from the standard AMIP (Atmospheric Model Intercomparison Project) SST data set at T42 resolution (Gates 1992), the same as those used in many previous studies (Sun and Trenberth 1998; Sun et al. 2003; Sun et al. 2006; Zhang and Sun 2006). The four models analyzed here are CCM3 (CAM1) (Kiehl et al. 1998), CAM2 (Kiehl and Gent, 2004), CAM3 at standard resolution, and CAM3 at T85 (Collins et al. 2006; Hack et al. 2006). The model data are from the AMIP runs of the four models that have the same SST forcing as observations.

3. Results

Figure 1 shows the spatial pattern of the response of clear-sky greenhouse effect in ERBE observations, NCEP reanalysis, and in the models. All the models simulate the observed positive response from the greenhouse effect of water vapor including the location of the maximum response over the central Pacific. The overestimate of the magnitude of the response in the models is also evident. Averaged over the immediate region of El Niño warming (160^{o}E-290^{o}E, 5^{o}S-5^{o}N), the response of greenhouse effect is 6.37 $Wm^{-2}K^{-1}$ in ERBE observations and 6.84 $Wm^{-2}K^{-1}$ in NCEP data, while the response in four models is respectively 8.26 $Wm^{-2}K^{-1}$ (CAM1), 8.17 $Wm^{-2}K^{-1}$ (CAM2), 8.33 $Wm^{-2}K^{-1}$ (T42 CAM3) and 8.65 $Wm^{-2}K^{-1}$ (T85 CAM3). So all the models have an excessive response in clear-sky greenhouse effect over the immediate region of El Niño warming and this excessive response is more severe in the T85 CAM3.

The differences in the response of greenhouse effect between the model simulations and ERBE observations could be in part due to the sampling differences between ERBE and the model data (Zhang et al. 1994; Allan and Ringer 2003; and Sohn et al. 2006), since regional differences in clear-sky OLR due to model-satellite sampling differences can reach 10~15 Wm^{-2}. But the bias due to the inadequate sampling does not explain the large range in the discrepancy as the models also overestimate the response compared to NCEP data (Figure 1). Note that these values presented here are the results of regional response. An early study of Soden (1997) concluded that the response of the tropical mean greenhouse effect of water vapor to El Niño warming in the GFDL model has a

close match with that from ERBE observations. We have to note, however, that the tropical mean signal of greenhouse effect associated with ENSO is much weaker than the signal averaged over the equatorial cold-tongue region of concern due to cancellations between different regions. The mean response of greenhouse effect averaged over the entire domain (120^oE-290^oE, 30^oS-30^oN) is respectively 0.79 $Wm^{-2}K^{-1}$ for ERBE observations, 1.04 $Wm^{-2}K^{-1}$ for CAM1, 0.77 $Wm^{-2}K^{-1}$ for CAM2, 1.00 $Wm^{-2}K^{-1}$ for CAM3 at T42, and 1.17 $Wm^{-2}K^{-1}$ for CAM3 at T85 resolution. So all the models overestimate the response only over the region of immediate warming, where the cause of this overestimate is our concern here. Why errors in moist regions tend to cancel those in the dry regions, however, is an interesting question, and will be investigated in a separate paper.

The clear-sky greenhouse effect is associated with the radiative effect of water vapor since water vapor absorbs the clear-sky outgoing longwave radiation (OLR), and results in a decrease in OLR. As shown in Shine and Sinha (1991) and Sun and Lindzen (1993), one percent change of water vapor in the upper troposphere can contribute to changes in the greenhouse effect as much as one percent change of water vapor in the lower troposphere, even though the corresponding absolute change in the absolute amount of water vapor is smaller by several magnitudes in the upper troposphere than in the lower troposphere. This is because the effectiveness of water vapor as a tropospheric greenhouse gas increases rapidly with height due to the decrease of temperature with

altitude (Schmetz et al. 1995). Figure 2 shows the percentage water vapor response at different levels of the troposphere, averaged over the immediate region of El Niño warming (160^{o}E-290^{o}E, 5^{o}S-5^{o}N). In both models and NCEP reanalysis, the response increases with height to about 500-400 mb, then decreases with height further up. (Note that NCEP has no data above 300 mb, so only the response below this level is plotted). The model-data discrepancy in the response of water vapor is small in the low troposphere, but large in the middle and upper troposphere. In the middle troposphere (600-500mb), ERA-40 reanalysis gives a consistent picture with NCEP data, although above 500 hPa, the response in ERA-40 is closer to that in the models than that in NCEP. At low troposphere around 850 hPa, the response in ERA-40 doubles that in NCEP. This suggests that in response to changes in SST, ERA-40 has high variability than NCEP for the precipitable water—the column-integrated water vapor amount, consistent with the findings of Trenberth et al. (2005). The difference in the response of water vapor is likely related to the different assimilation technique used in these two reanalyses. The NCEP reanalysis did not assimilate the special sensor microwave imager (SSM/I) water vapor data or utilize the water vapor infrared channels, while ERA-40 reanalysis uses the water vapor channels from TIROS operational vertical sounder (TOVS) and ATOVS as well as SSM/I radiances (Trenberth et al. 2005).

Figure 3 further shows a comparison of the vertical profile of the temperature response between two reanalysis data and the models. The discrepancy in the

temperature response between models and two reanalysis data at all tropospheric levels is within 0.3 K/K. The maximum discrepancy in the temperature response occurs in the immediate neighborhood of 600 mb. The response of temperature in the middle troposphere is weaker in the models than that from the reanalysis data. The cause for this underestimate in the middle troposphere is that the cold phase is generally warmer in the models than in the reanalysis (not shown here). Note that the temperature response in both models and reanalyses shows a minimum in the mid-troposphere and a maximum in the upper troposphere around 300 hPa and in the near surface. This indicates a strong coupling between SST and temperature in the near surface and upper troposphere. This vertical structure is consistent with the lapse rate model of Sun and Lindzen (1993). The upper troposphere is the levels where deep convection detrains (see also Wu et al. 2006; Folkins and Martin 2005). Since an air parcel ascending in the deep convective towers conserves its enthalpy, the upper tropospheric temperature is effectively coupled to the boundary layer moist enthalpy and thereby to the SST. As the detrained air descends, it loses heat to space radiatively and gradually loses its memory and therefore its coupling with the surface property.

To obtain a quantitative measure of the relative contributions to the errors in the clear-sky greenhouse effect from the bias in the response of temperature and the bias in the response of water vapor, we have employed a radiation model (Chou 1986), the same radiation routine used in Sun and Lindzen (1993), to calculate the differences in the greenhouse effect due to different temperature or water vapor profiles. To estimate the

contributions from the differences in the lapse rate response to the differences in the clear-sky greenhouse effect response, we first use the annual mean vertical profile of water vapor and temperature from NCEP reanalysis over the region of El Niño warming (160^{o}E-290^{o}E, 5^{o}S-5^{o}N) to calculate the mean clear-sky greenhouse effect as a reference value of greenhouse effect. We then add to the reference profiles of temperature the temperature response from NCEP data and models shown in Fig.3, for a 1 K increase in the SST. We keep the water vapor profile fixed unchanged in the calculation of greenhouse effect. We then contrast the differences between greenhouse effect from the changed temperature profile and greenhouse effect from the case with the reference temperature profile. Similarly, to estimate the contributions from the differences in the water vapor response to the differences in the clear-sky greenhouse effect, we keep the temperature profile fixed to the NCEP reference profile, but add to the reference profile for water vapor the response of water vapor for a 1 K increase in the SST (Fig.2). To quantify the combined contributions from the differences in the water vapor response and the differences in the temperature response to the differences in the response of greenhouse effect, we add to both profiles of water vapor and temperature their corresponding changes for a 1 K increase in the SST as shown in Fig. 2 and Fig. 3. The results from these calculations are summarized in Table 1. Clearly, the differences in the water vapor response explain the bulk of the differences in the response of greenhouse effect. The contribution from the differences in the temperature response is secondary. Note that the discrepancies in greenhouse effect do not exactly match the contributions

due to the combined effect. This small discrapancy is expected because in our calculation, we have fixed the humidity above 300 mb constant—we do not have data from NCEP above this level. It is quite possible that the models are also moister than NCEP data in the layer between 300 mb and the tropopause, given that they are moister than NCEP data in the bulk of the upper troposphere where we have data to compare with. The contribution from the interannual variability of CO2 is small. As shown in Keeling et al. (1995), the increase in CO2 concentration associated with ENSO during the ERBE period is around 1 ppm. Its contribution to the radiative forcing is only 0.014 Wm^{-2} through the off-line calculation with the radiation code. The corresponding results from using ERA-40 reanalysis as reference profile lead to the same conclusions.

Compared to NCEP reanalysis, the models in the upper troposphere tend to be moister in regions of ascending motion and drier in regions of descending motion. The left column of Figure 4 shows the differences of water vapor between model simulations and the NCEP reanalysis (shaded in red and blue) and the differences of vertical velocity between model simulations and NCEP reanalysis (dashed and solid contours). The figure shows that above the trade wind boundary layer, there is a good spatial correlation between the sign of the bias in water vapor and the sign of the bias in the mean vertical motion. The ascending motion over the western Pacific is much stronger in the models than in NCEP data. The upper troposphere over that region is much moister in the models than in the NCEP reanalysis. The strength of the vertical motion over the eastern Pacific is also stronger in the model simulations than in the reanalysis, although the bias

is not as strong as that in the western Pacific. Correspondingly, the upper troposphere in that region is also somewhat drier. The models have a stronger ascending motion and more moisture compared to NCEP reanalysis in regions with deep convection—the western Pacific warm-pool and the ITCZ (intertropical convergence zone) that is north to the equator in the eastern Pacific (Figures 4f-4j). It is clear that deep convection in the models delivers too much moisture to the upper troposphere. As the deep convection shifts to the central Pacific during El Niño, it results in an excessive response of water vapor in the upper troposphere in that region which is already somewhat drier because of the stronger descending motion induced by the stronger ascending motion in the western Pacific, where the deep convection is originally concentrated. The response of the vertical motion to ENSO in the models is also stronger than that in the NCEP reanalysis. Figure 5 shows a basin view of the response of vertical motion to the SST increase in the central Pacific during El Niño warming. The vertical velocity only changes slightly in the western Pacific warm pool, indicating that the ascending motion is still very strong during El Niño warming. The largest change in vertical velocity is located in the central Pacific where the largest change in the water vapor occurs. Figure 6 gives the vertical cross sections of the changes in water vapor and vertical velocity in response to ENSO. The figure reinforces the impression from Fig. 4 about the spatial correlation between the vertical velocity and the upper tropospheric water vapor. The dry bias in the mean over the central Pacific shown in Figure 4 becomes a wet bias during El Niño warming (left column of Fig 6), and this wet bias is accompanied with a stronger response of vertical

motion (right column of Fig.6).

To further quantify the relative contributions to the discrepancy in the water vapor response from the two phases of ENSO, we have performed composite analysis of the water vapor anomaly during the warm and cold phases. The results indicate that the models are not only too moist in the warm periods (Figure 7a) but too dry in the cold periods over the equatorial Pacific cold-tongue region (Figure 7b). The drier bias shown in Fig.4 is thus mainly from the bias in the cold phase. Fig.7cd further shows the composite of the anomalous vertical motion in the models for the two phases of ENSO. The figures show that the models' vertical motion is more sensitive to El Niño warming (Figure 7c) and to La Niña cooling (Figure 7d) than those in the NCEP reanalysis, except that above 600hPa the response of vertical motion in CAM2 and CAM3 is slightly less sensitive than NCEP, which is due to a shift off the equator of the maximum response in these two models shown in the right panel of Figure 5. The models appear to have a greater bias of water vapor during the warm phase than in the cold phase.

The excessive response of water vapor in the models is also linked to the bias in the response of upper cloud cover (Figure 8a). We have noted that all the models overestimate the upper cloud cover response compared to ISCCP data. The overestimate of water vapor response in the upper troposphere is about 8%/K ~20%/K, and the associated upper cloud cover response is overestimated by about 5%/K in CCM3 and about 3%/K in three latest versions. The response of vertical motion over the region of

concern is shown in Figure 8b. The results strengthen the impression that the models have higher sensitivity to SST forcing in the vertical motions in the low and middle troposphere. It is clear that in the models the excessive response of upper tropospheric water vapor is associated with an excessive response in the vertical motion and upper cloud cover. Further research is needed to establish whether the stronger vertical motion is a cause or a consequence of the excessive upper level cloud amount and humidity.

4. Summary

To better understand the causes of the overestimate in the response of clear-sky greenhouse effect to El Niño warming over the region of warming in four Community Atmosphere Models, the response of water vapor and temperature to El Niño warming is examined as a function of height. Consistent with the results from the NCEP reanalysis, all the models, measured by percentage change, have a stronger water vapor response to the surface ocean warming in the middle to upper troposphere than in the lower troposphere. However, the water vapor response in the middle to upper troposphere in the models is considerably stronger than in the NCEP reanalysis. The temperature response in contrast is weaker in the models in the middle troposphere (the level around 600 mb). These biases are also revealed by comparing the model simulations and ERA-40 reanalysis.

Utilizing a radiation model, the data-model discrepancy in the temperature response is

found to contribute little to the bias of greenhouse effect. The difference in the temperature response only accounts for about 10% of the bias in the response of greenhouse effect. The overestimate in the response of greenhouse effect is mostly due to an overestimate of the response in the middle to upper tropospheric water vapor.

The models have more moisture in the upper troposphere in regions of deep convection—the western Pacific. Accompanied with this bias in moisture is a much stronger ascending motion in regions of deep convection. The models also have a drier bias in regions of descending motion—the central and eastern Pacific, although it is less severe than the moist bias in regions with deep convection. Consistent with the stronger ascending motion in the western Pacific, the descending motion in the eastern and central Pacific is also stronger in the models.

Further analysis reveals that compared to the NCEP reanalysis, the excessive response of water vapor in the models is due to the bias that the models are too moist in warm periods and too dry in cold periods. The bias in warm periods is greater than that in cold periods. The models have a stronger vertical motion that is more sensitive to El Niño warming and La Niña cooling than the reanalysis. When deep convection shifts to the central equatorial Pacific during El Niño warming, the normally drier bias becomes a wet bias as the deep convection moistens the upper troposphere in the models too much. This is consistent with an excessive response in the upper cloud cover. There is a good spatial correlation between the bias in the moisture and the bias in the vertical motion. Whether the bias in the vertical motion is the cause of the bias in the moisture or the bias

in the moisture causes the bias in the vertical motion will be investigated in the future research. For now, we note that there could be a positive feedback loop that links the bias in the vertical motion and the bias in the upper tropospheric moisture. Recall that an excessive trapping of infrared energy from excessive upper level moisture will likely enhance the vertical motion (Ramanathan and Collins 1991). Similarly, a drier upper troposphere may increase the radiative cooling in the mid troposphere and correspondingly increase the strength of the descending motion (Sun and Lindzen 1993; Betts and Ridgeway 1989).

Following the analysis of Sun et al. (2001), we have examined the correlation between the upper tropospheric humidity variations and those at the surface level over the tropics, and found that this correlation is higher in the models than in the reanalysis (Not shown here). Therefore a possible excessive background diffusion in the models continues to be a concern. We also note that in the middle troposphere, two CAM3 models have a comparable cloud response to El Niño warming but they have an excessive water vapor response (the overestimate is about 20%/K). Interestingly, for the other two models, the water vapor response is also considerably larger in the middle troposphere but the middle cloud response is apparently underestimated. This again highlights the fact that we do not yet know well the relationship between clouds and humidity, and more generally the precipitation efficiency of tropical convection. With new satellite data from "A Train" (Stephens et al. 2002), we may be in a better position to address these critical climate issues.

The bias of the excessive response of clear-sky greenhouse effect to ENSO forcing is not a special problem in Community Atmosphere Models, it also exists in other models (Sun et al. 2006; Sun et al. 2007). The present analysis on the Community Atmosphere Models may hold a key to better understanding the cause for the bias in other models. We plan to extend the analysis to all the new generation models participated in the Intergovernmental Panel on Climate Change (IPCC) Fourth Assessment Report (AR4) in a separate study.

Acknowledgement

This research was supported by NOAA's Climate Dynamics and Environmental Prediction Program, and by NSF's climate dynamics program under ATM-9912434, ATM-0331760, ATM-0553111, and ATM-0602488. The authors would like to thank Dr. James J. Hack and Dr. Jeff Kiehl of NCAR for providing us the outputs from T85 CAM3.

References

Allan, R. P., and M. A. Ringer, 2003: Inconsistencies between satellite estimates of longwave cloud forcing and dynamical fields from reanalyses, *Geophys. Res. Lett.*, 30(9), 1491, doi:10.1029/2003GL017019.

Barkstrom, B. R., 1984: The Earth Radiation Budget Experiment (ERBE), *Bull. Am. Meteorol. Soc.*, *65*, 1170–1185.

Betts, A. K. and W. Ridgway, 1989: Climatic equilibrium of the atmospheric convective boundary layer over a tropical ocean. J. Atmos. Sci., **46**, 2621-2641.

Boer G. J., B. Yu, S.-J. Kim, and G. M. Flato, 2004: Is there observational support for an El Niño-like pattern of future global warming? *Geophys. Res. Lett.*, **31**, L06201, doi:10.1029/2003GL018722.

Cai W., and P. H. Whetton, 2000: Evidence for a time-varying pattern of greenhouse warming in the Pacific Ocean. *Geophys. Res. Lett.*, **27**, 2577–2580.

Chou, M. D., 1986: Atmospheric solar heating rate in water vapour bands. *J. Climate Appl. Meteor.,* **25**, 1532-1542.

Collins, W. D., P. J. Rasch, B. A. Boville, J. J. Hack, J. R. McCaa, D. L. Williamson, B. P. Briegleb, C. M. Bitz, S.-J. Lin, and M. H. Zhang, 2006: The formulation and atmospheric simulation of the Community Atmosphere Model version 3 (CAM3), J. Clim., **19**, 2144–2161.

Folkins, I., and R. V. Martin, 2005: The vertical structure of tropical convection and its

impact on the budgets of water vapor and ozone, J. Atmos. Sci., **62**, 1560-1573.

Gates, W. L., 1992: AMIP: The Atmospheric Model Intercomparison Project. *Bull. Amer. Meteor. Soc.,* **73,** 791–794.

Hack, J. J., J. M. Caron, G. Danabasoglu, K. W. Oleson, C. M. Bitz, and J. E. Truesdale, 2006: CCSM-CAM3 climate simulation sensitivity to changes in horizontal resolution, J. Clim., 19, 2267–2289.

Held, I. M. and B. J. Soden, 2000: Water vapor feedback and global warming. *Ann. Rev. Energy Environ*., **25**, 441-475.

Houghton J. T., Y. Ding, D. J. Griggs, M. Noguer, P. J. van der Linden, X. Dai, K. Maskell, and C. A. Johnson, 2001: *Climate Change 2001: The Scientific Basis*. Cambridge University Press, 881 pp.

Inamdar, A. K., and V. Ramanathan**,** 1994: Physics of greenhouse effect and convection in warm oceans. *J. Clim.,* **7**, 715-731.

Kalnay, E., and Coauthors, 1996: The NCEP/NCAR 40-Year Reanalysis Project. *Bull. Amer. Meteor. Soc.,* **77**, 437–471.

Keeling, C. D., T. P. Whorf, M. Wahlen, J. van der Plicht, 1995: Interannual extremes in the rate of rise of atmospheric carbon dioxide since 1980. *Nature,* **375**, 666-670.

Kiehl, J. T., and K. E. Trenberth, 1997: Earth's annual global mean energy budget. *Bull. Amer. Meteor. Soc.,* **78**, 197–208.

Kiehl, J. T., J. J. Hack, G. Bonan, B. A. Boville, D. Williamson, and P. J. Rasch, 1998: The National Center for Atmospheric Research Community Climate Model: CCM3, J.

Clim., 11, 1131–1149.

Kiehl, J. T., and P. R. Gent, 2004: The Community Climate System Model, version two, J. Clim., 17, 3666–3683.

Meehl G. A., and W. M. Washington, 1996: El Niño-like climate change in a model with increased atmospheric CO_2 concentrations. *Nature*, **382**, 56–60.

Ramanathan, V., and W. Collins, 1991: Thermodynamic regulation of ocean warming by cirrus clouds deduced from observations of the 1987 El Niño, Nature, 351, 27–32.

Raval, A., and V. Ramanathan, 1989: Observational determination of the greenhouse effect, Nature, 342, 758–762.

Rossow, W. B., and R. A. Schiffer, 1999: Advances in understanding clouds from ISCCP, Bull. Am. Meteorol. Soc., 80, 2261–2288.

Rossow, W. B., A. W. Walker, D. E. Beuschel, and M. D. Roiter, 1996: International Satellite Cloud Climatology Project (ISCCP) documentation of new cloud datasets, Rep. WMO/TD-737, 115 pp., World Meteorol. Organ., Geneva, Switzerland.

Schmetz, J., W. P. Menzel, C. Velden, X. Wu, L. van de Berg, S. Nieman, C. Hayden, K. Holmlund, and C. Geijo, 1995: Monthly mean large-scale analyses of upper-tropospheric humidity and wind field divergence derived from three geostationary satellites, Bull. Amer. Meteor. Soc., **76**, 1578-1584.

Shine, K. P., and A. Sinha, 1991: Sensitivity of the earth's climate to height-dependent changes in the water vapor mixing ratio. *Nature*, **354**, 382-384.

Soden, B. J.**,** 1997: Variations in the tropical greenhouse effect during El Niño, *J. Clim.*,

10, 1050–1055.

Sohn, B.-J., J. Schmetz, R. Stuhlmann, and J.-Y. Lee, 2006: Dry Bias in Satellite-Derived Clear-Sky Water Vapor and Its Contribution to Longwave Cloud Radiative Forcing, *J. Clim.*, **19**, 5570–5580.

Stephens G. L, Coauthors, 2002: The Cloudsat Mission and the A-Train. *Bull. Amer. Meteor. Soc.*, **83**, 1771–1790.

Stocker, T. F., and Coauthors, 2001: Physical climate processes and feedbacks. *Climate Change 2001: The Scientific Basis* (Contribution of Working Group I to the Third Assessment Report of the Intergovernmental Panel on Climate Change). J. T. Houghton et al., Eds., Cambridge University Press, 417-470.

Sun, D.-Z., and R. S. Lindzen, 1993: Water vapor feedback and the ice age snowline record. *Ann. Geophys.*, **11**, 204-215.

Sun D.-Z., and I. Held, 1996: A comparison of modeled and observed relationships between interannual variations of water vapor and temperature. *J. Climate*, **9**, 665–675.

Sun, D.-Z., and K. E. Trenberth, 1998: Coordinated heat removal from the equatorial Pacific during the 1986–87 El Niño, Geophys. Res. Lett., 25, 2659–2662.

Sun, D.-Z., C. Covey, and R. S. Lindzen, 2001: Vertical correlations of water vapor in GCMs, *Geophys. Res. Lett.*, *28*, 259–262.

Sun, D.-Z., J. Fasullo, T. Zhang, and A. Roubicek, 2003: On the radiative and dynamical feedbacks over the equatorial cold-tongue. *J. Clim.*, **16**, 2425-2432.

Sun, D.-Z., T. Zhang, C. Covey, S. A. Klein, W. D. Collins, J. J. Hack, J. T. Kiehl, G. A.

Meehl, I. M. Held, and M. Suarez, 2006: Radiative and Dynamical Feedbacks Over the Equatorial Cold-tongue: Results from Nine Atmospheric GCMs. *J. Clim.*, **19**, 4059-4074.

Sun, D.-Z., Y. Yu, and T. Zhang, 2007: Tropical water vapor and cloud feedbacks in climate models: a further assessment using coupled simulations. *J. Clim.* (Submitted).

Timmerman A. J., J. Oberhuber, A. Bacher, M. Esch, M. Latif, and E. Roeckner, 1999: Increased El Niño frequency in a climate model forced by future global warming. *Nature*, **398**, 694–696.

Trenberth, K. E., J. Fasullo, and L. Smith, 2005: Trends and variability in column-integrated atmospheric water vapor, Clim. Dyn., 24, 741–758.

Uppala, S. M., et al., 2005: The ERA-40 reanalysis, Q. J. R. Meteorol. Soc., 131, 2961–3012, doi:10.1256/qj.04.176/.

Wu, W., A. E. Dessler, and G. R. North, 2006: Analysis of the correlations between atmospheric boundary-layer and free-tropospheric temperatures in the tropics, Geophys. Res. Lett., 33, L20707, doi:10.1029/2006GL026708.

Zhang M. H., R. D. Cess, T. Y. Kwon, and M. H. Chen, 1994: Approaches of comparison for clear-sky radiative fluxes from general circulation models with Earth Radiation Budget Experiment data. *J. Geophys. Res.*, **99**, 5515–5523.

Zhang, T. and D.-Z. Sun, 2006: Response of water vapor and clouds to El Niño warming in three National Center for Atmospheric Research atmospheric Models. *J. Geophys. Res.*, **111**, D17103, doi:10.1029/2005JD006700.

Table captions

Table 1: The discrepancy with ERBE observations and NCEP reanalysis (the numbers in parentheses) in the response of clear-sky greenhouse effect and the contributions to this discrepancy due to the errors in temperature and humidity response in the models with respect to NCEP reanalysis over the region of El Niño warming (160^{o}E-290^{o}E, 5^{o}S-5^{o}N). The contributions to greenhouse effect discrepancy are calculated as the differences in the response of greenhouse effect to 1K SST increase between models and the same NCEP reference value for each case (see text for details). The numbers in parentheses listed in the last three columns of the table are the contributions to greenhouse effect discrepancy estimated from the results using ERA-40 reanalysis as reference value.

Figure captions

Figure 1: Response of the clear-sky greenhouse effect to El Niño warming from (a) ERBE observations, (b) NCEP reanalysis, (c) CAM1, (d) CAM2, (e) T42 CAM3, and (f) T85 CAM3. Shown are regression coefficients obtained by linearly regressing the clear-sky greenhouse effect at each grid point against the underlying SST averaged over the region of El Niño warming (160^{o}E-290^{o}E, 5^{o}S-5^{o}N). The interannual variations of greenhouse effect over the ERBE period are used for the calculations.

Figure 2: Percentage response of specific humidity to El Niño warming as a function of height from the NCEP-NCAR reanalysis, ERA-40 reanalysis, and four models averaged over the equatorial Pacific (160^{o}E-290^{o}E, 5^{o}S-5^{o}N). Shown are regression coefficients divided by the respective climatology. In every vertical level, the regression coefficients are obtained by linearly regressing specific humidity at the corresponding level against the underlying SST (as in Figure 19 of Zhang and Sun [2006]) averaged over the region of El Niño warming (160^{o}E-290^{o}E, 5^{o}S-5^{o}N). The interannual variations of specific humidity over the ERBE period are used for the regression calculations.

Figure 3: Response of air temperature to El Niño warming as a function of height from

the NCEP-NCAR reanalysis, ERA-40 reanalysis, and four models averaged over the equatorial Pacific (160^{o}E-290^{o}E, 5^{o}S-5^{o}N). Shown in every vertical level are regression coefficients obtained by linearly regressing the air temperature at the corresponding level against the underlying SST averaged over the region of El Niño warming (160^{o}E-290^{o}E, 5^{o}S-5^{o}N). The interannual variations of air temperature over the ERBE period are used for the regression calculations.

Figure 4: The vertical cross sections of annual mean vertical velocity averaged over the equator (5^{o}S-5^{o}N) from NCEP data and the difference between models and NCEP data (left panel) and spatial patterns at 400 hPa (right panel) for annual mean vertical velocity from NCEP reanalysis and four models over the ERBE period. The shaded values in (b-e) and (g-j) are the percentage differences in annual mean specific humidity between the models and NCEP data over the same period. They are obtained from the differences between models and NCEP data divided by the values of NCEP data.

Figure 5: The spatial pattern of the response of vertical velocity to El Niño warming at 850 hPa (left panel) and at 500 hPa (right panel) from the NCEP-NCAR reanalysis and four models. Shown are regression coefficients obtained by linearly regressing vertical velocity against the underlying SST averaged over the region of El Niño warming (160^{o}E-290^{o}E, 5^{o}S-5^{o}N). The interannual variations of vertical velocity over the ERBE period are used for the regression calculations.

Figure 6: The vertical cross sections averaged over the equator (5^oS-5^oN) for the percentage response of specific humidity (left panel) and the response of vertical velocity (right panel) to El Niño warming from NCEP data and four models. Shown in every vertical level are the responses obtained by the same way as in Figure 2 and Figure 5.

Figure 7: The composite percentage changes in specific humidity during (a) warm periods and (b) cold periods as a function of height from the NCEP-NCAR reanalysis and four models averaged over the equatorial Pacific (160^oE-290^oE, 5^oS-5^oN). The percentage changes in specific humidity are calculated as the anomalies divided by the respective climatology. Also shown are the composite changes in vertical velocity during (c) warm periods and (d) cold periods as a function of height from the NCEP-NCAR reanalysis and four models averaged over the equatorial Pacific (160^oE-290^oE, 5^oS-5^oN). The warm and cold periods are defined as the periods when the Niño-3 SST anomalies are larger than 0.3^oC and less than -0.3^oC over the ERBE period, respectively.

Figure 8: Responses of (a) cloud cover from ISCCP observations and four models, and (b) vertical velocity from the NCEP reanalysis and four models to El Niño warming as a function of height averaged over the equatorial Pacific (160^oE-290^oE, 5^oS-5^oN). The cloud cover data used here are the high, middle and low cloud cover (indicated by the markers shown in Fig.8a) for both models and observations, the same as those used by

Sun et al. (2003) and Zhang and Sun (2006). Shown in every vertical level are regression coefficients obtained by linearly regressing the concerned quantities at the corresponding level against the underlying SST averaged over the region of El Niño warming (160^{o}E-290^{o}E, 5^{o}S-5^{o}N). The interannual variations of the concerned quantities over the ERBE period are used for the regression calculations.

Table 1: The discrepancy with ERBE observations and NCEP reanalysis (the numbers in parentheses) in the response of clear-sky greenhouse effect and the contributions to this discrepancy due to the errors in temperature and humidity response in the models with respect to NCEP reanalysis over the region of El Niño warming (160^{o}E-290^{o}E, 5^{o}S-5^{o}N). The contributions to greenhouse effect discrepancy are calculated as the differences in the response of greenhouse effect to 1K SST increase between models and the same NCEP reference value for each case (see text for details). The numbers in parentheses listed in the last three columns of the table are the contributions to greenhouse effect discrepancy estimated from the results using ERA-40 reanalysis as reference value.

Model Names	discrepancy with ERBE and NCEP ($Wm^{-2}K^{-1}$)	contribution to the discrepancy ($Wm^{-2}K^{-1}$)		
		Lapse rate effect	Humidity effect	combined effect
CAM1	1.89 (1.42)	0.053 (0.071)	1.65 (1.48)	1.71 (1.56)
CAM2	1.80 (1.33)	0.31 (0.36)	0.87 (0.43)	1.21 (0.81)
CAM3	1.96 (1.49)	0.23 (0.27)	1.12 (0.74)	1.39 (1.04)
CAM3 (T85)	2.28 (1.81)	0.020 (0.039)	1.66 (1.40)	1.70 (1.46)

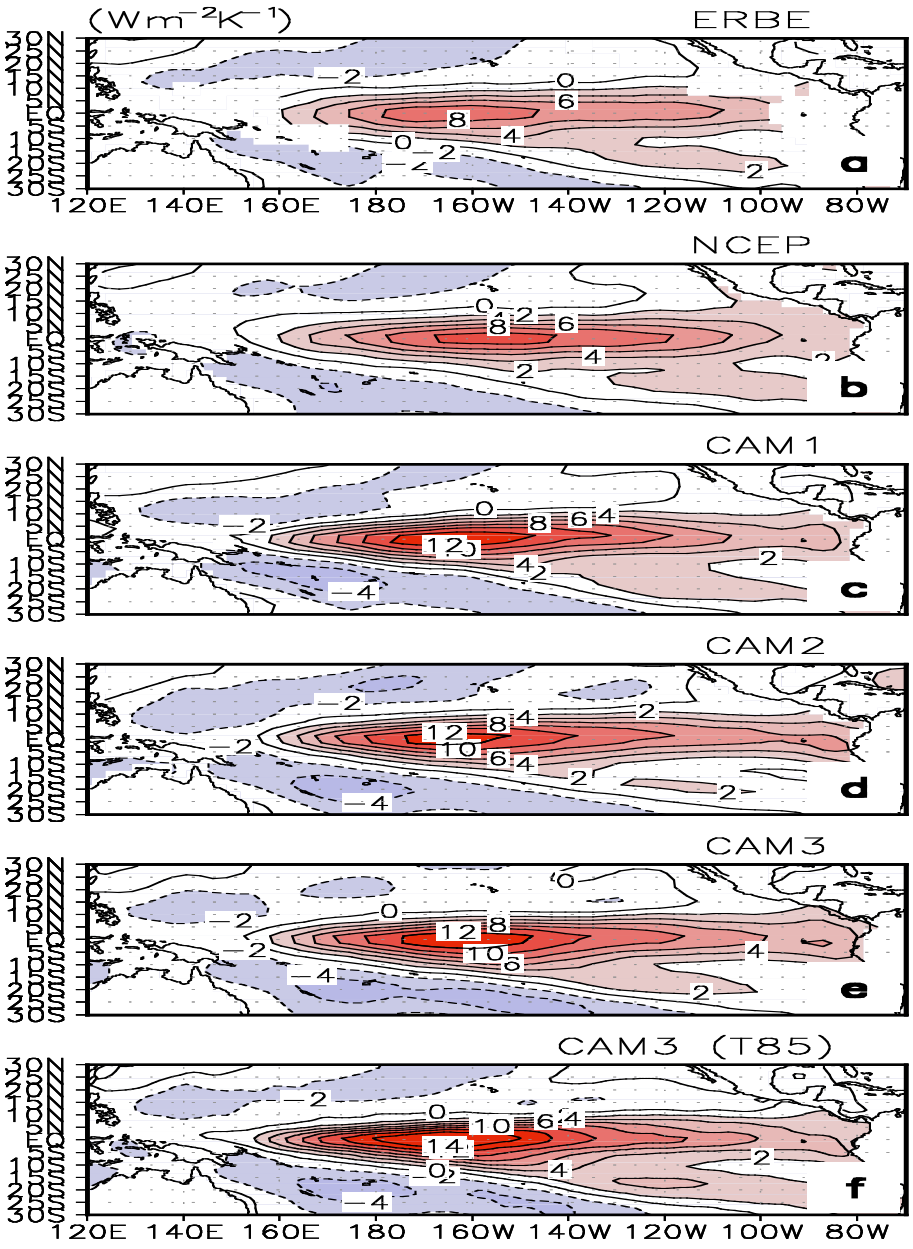

Figure 1: Response of the clear-sky greenhouse effect to El Niño warming from (a) ERBE observations, (b) NCEP reanalysis, (c) CAM1, (d) CAM2, (e) T42 CAM3, and (f) T85 CAM3. Shown are regression coefficients obtained by linearly regressing the clear-sky greenhouse effect at each grid point against the underlying SST averaged over the region of El Niño warming (160°E-290°E, 5°S-5°N). The interannual variations of greenhouse effect over the ERBE period are used for the calculations.

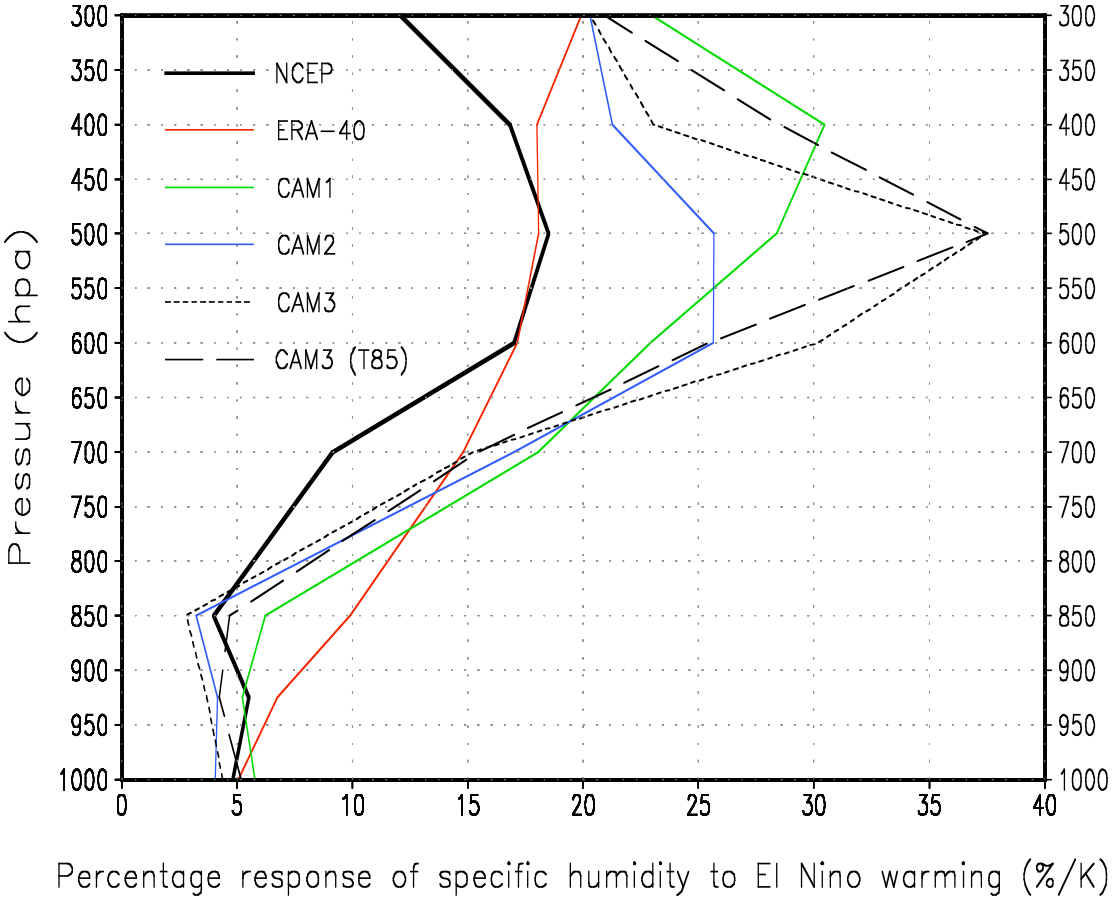

Figure 2: Percentage response of specific humidity to El Niño warming as a function of height from the NCEP-NCAR reanalysis, ERA-40 reanalysis, and four models averaged over the equatorial Pacific (160°E-290°E, 5°S-5°N). Shown are regression coefficients divided by the respective climatology. In every vertical level, the regression coefficients are obtained by linearly regressing specific humidity at the corresponding level against the underlying SST (as in Figure 19 of Zhang and Sun [2006]) averaged over the region of El Niño warming (160°E-290°E, 5°S-5°N). The interannual variations of specific humidity over the ERBE period are used for the regression calculations.

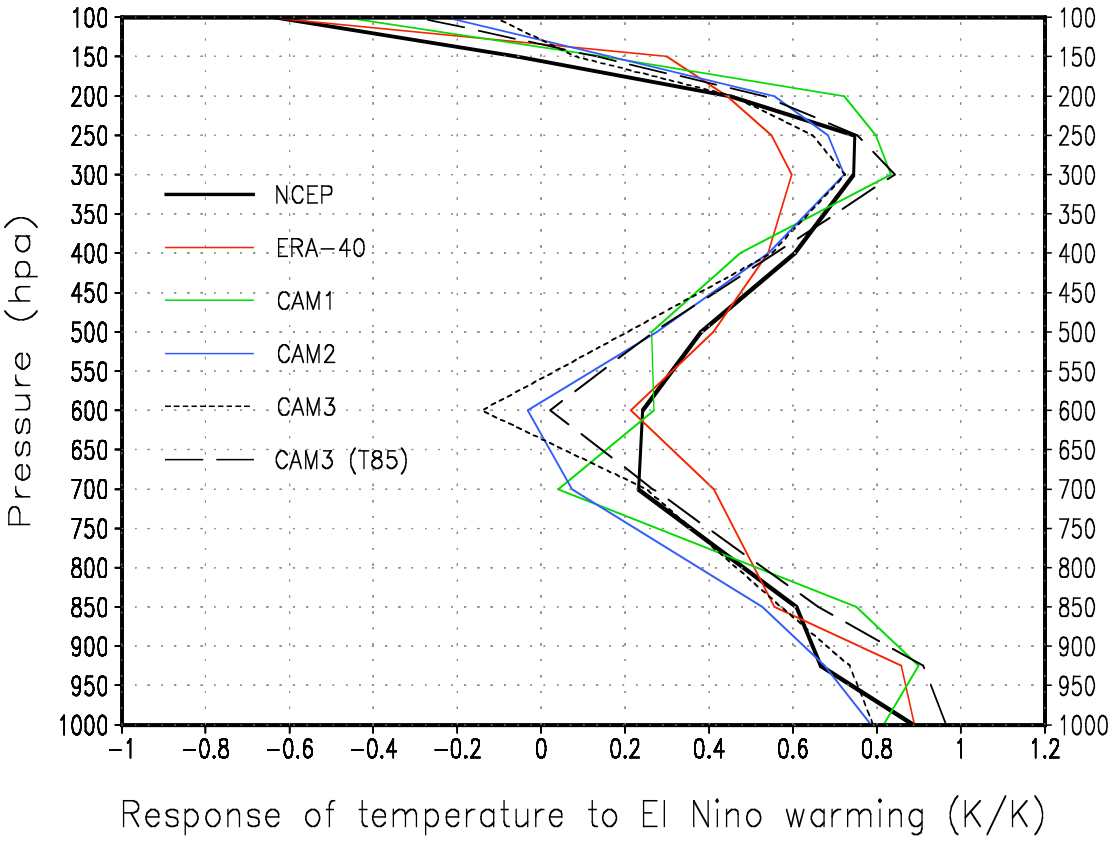

Figure 3: Response of air temperature to El Niño warming as a function of height from the NCEP-NCAR reanalysis, ERA-40 reanalysis, and four models averaged over the equatorial Pacific (160°E-290°E, 5°S-5°N). Shown in every vertical level are regression coefficients obtained by linearly regressing the air temperature at the corresponding level against the underlying SST averaged over the region of El Niño warming (160°E-290°E, 5°S-5°N). The interannual variations of air temperature over the ERBE period are used for the regression calculations.

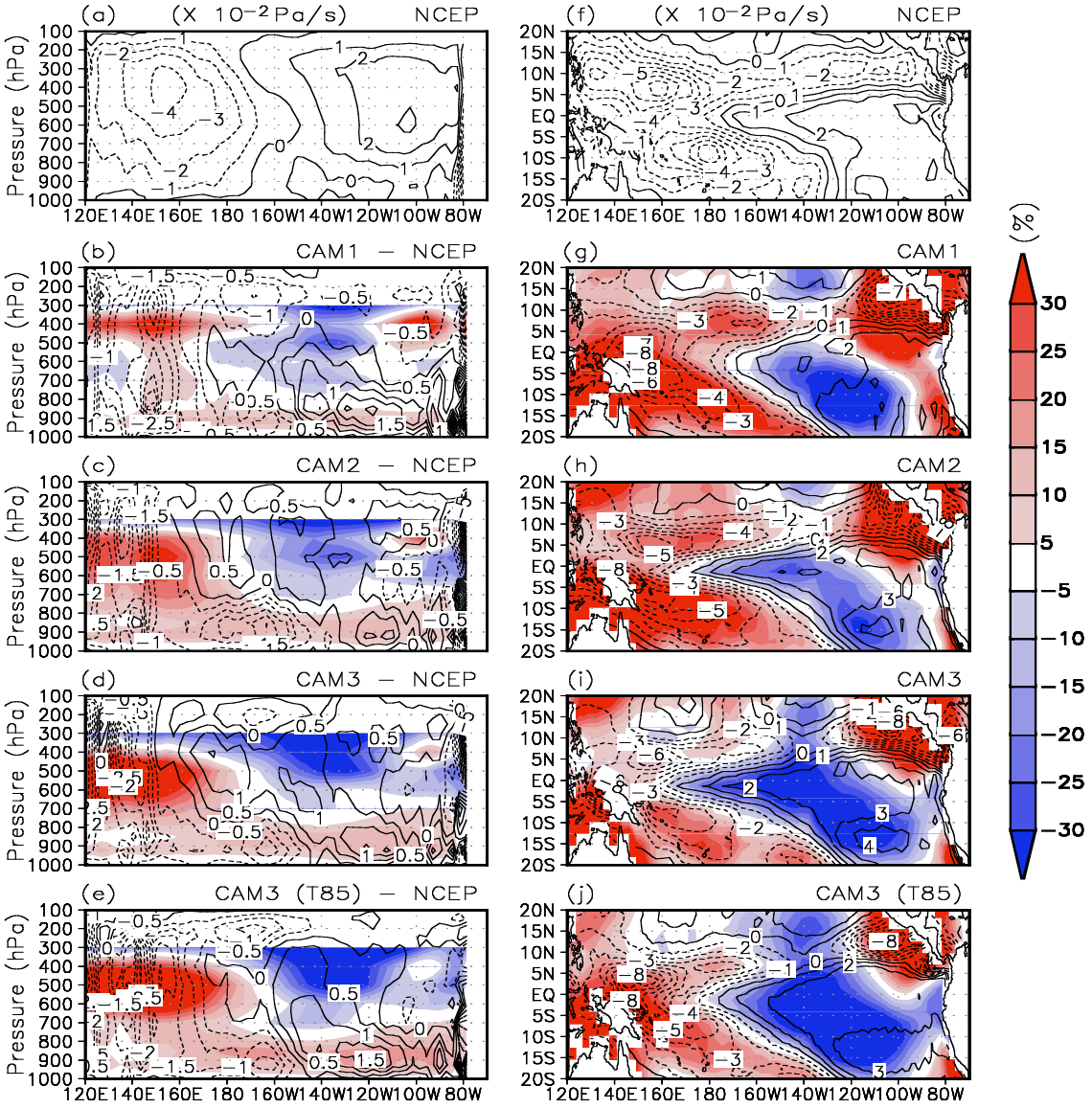

Figure 4: The vertical cross sections of annual mean vertical velocity averaged over the equator (5°S-5°N) from NCEP data and the difference between models and NCEP data (left panel) and spatial patterns at 400 hPa (right panel) for annual mean vertical velocity from NCEP reanalysis and four models over the ERBE period. The shaded values in (b-e) and (g-j) are the percentage differences in annual mean specific humidity between the models and NCEP data over the same period. They are obtained from the differences between models and NCEP data divided by the values of NCEP data.

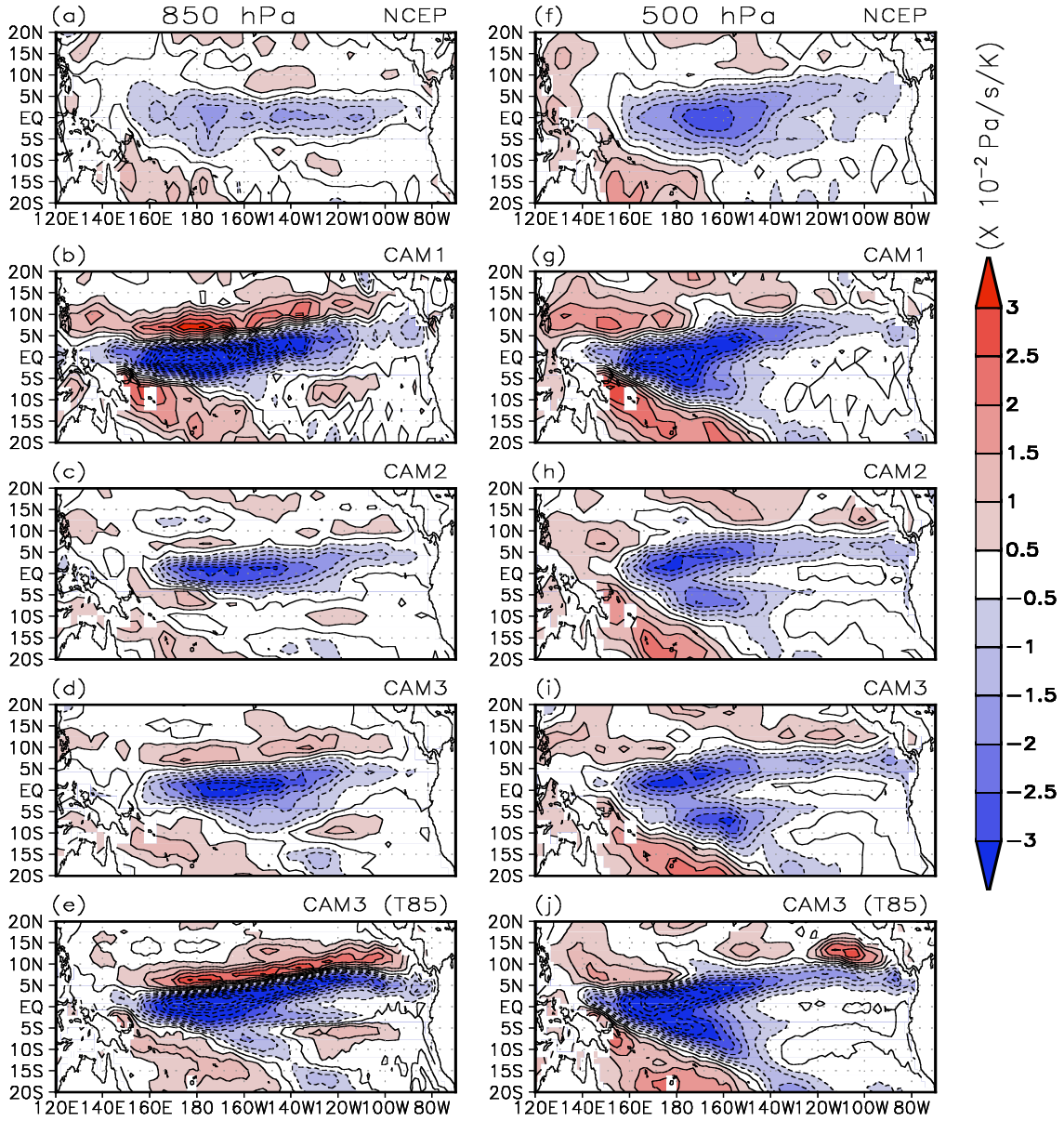

Figure 5: The spatial pattern of the response of vertical velocity to El Niño warming at 850 hPa (left panel) and at 500 hPa (right panel) from the NCEP-NCAR reanalysis and four models. Shown are regression coefficients obtained by linearly regressing vertical velocity against the underlying SST averaged over the region of El Niño warming (160°E-290°E, 5°S-5°N). The interannual variations of vertical velocity over the ERBE period are used for the regression calculations.

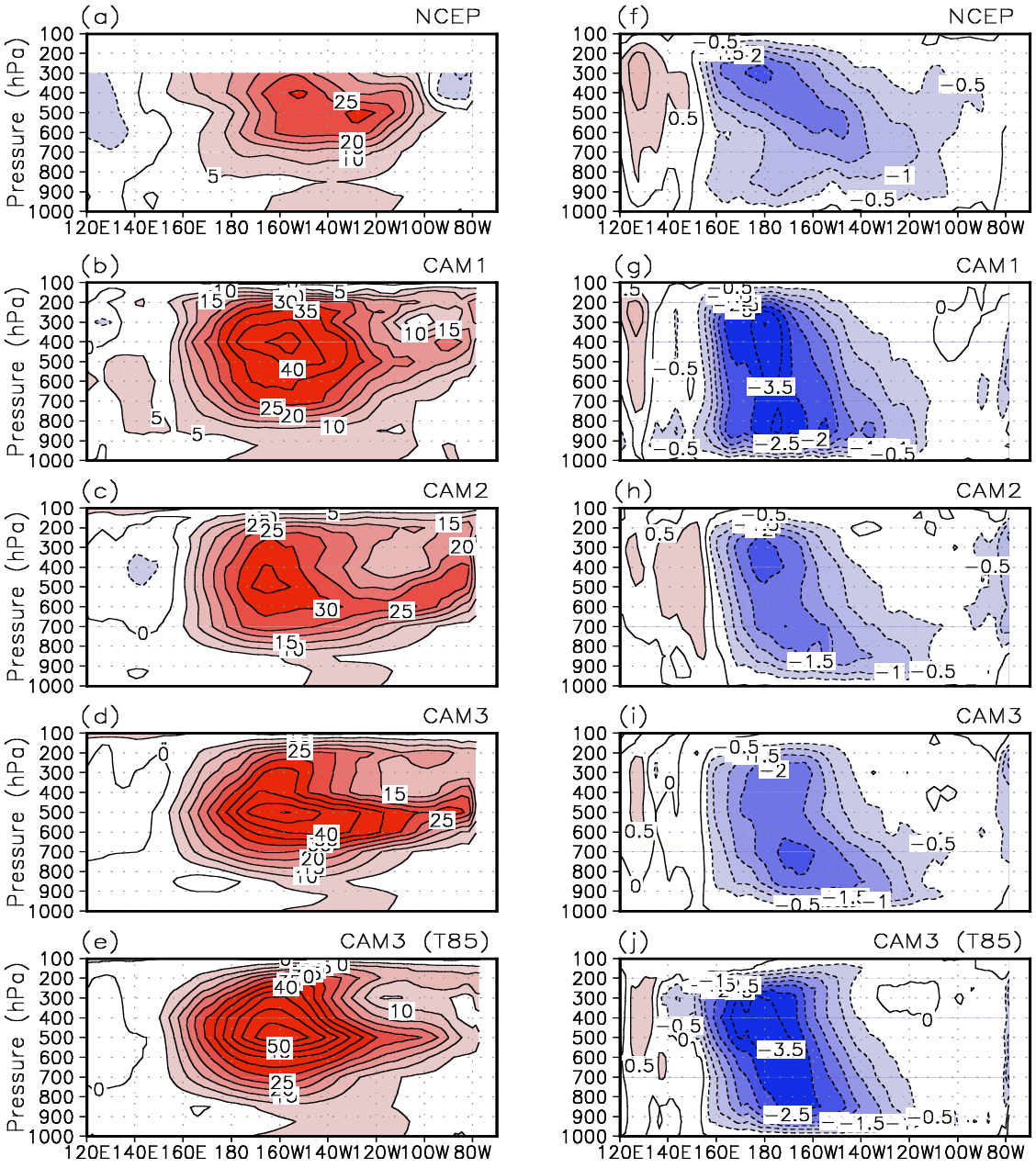

Figure 6: The vertical cross sections averaged over the equator (5^{o}S-5^{o}N) for the percentage response of specific humidity (left panel) and the response of vertical velocity (right panel) to El Niño warming from NCEP data and four models. Shown in every vertical level are the responses obtained by the same way as in Figure 2 and Figure 5.

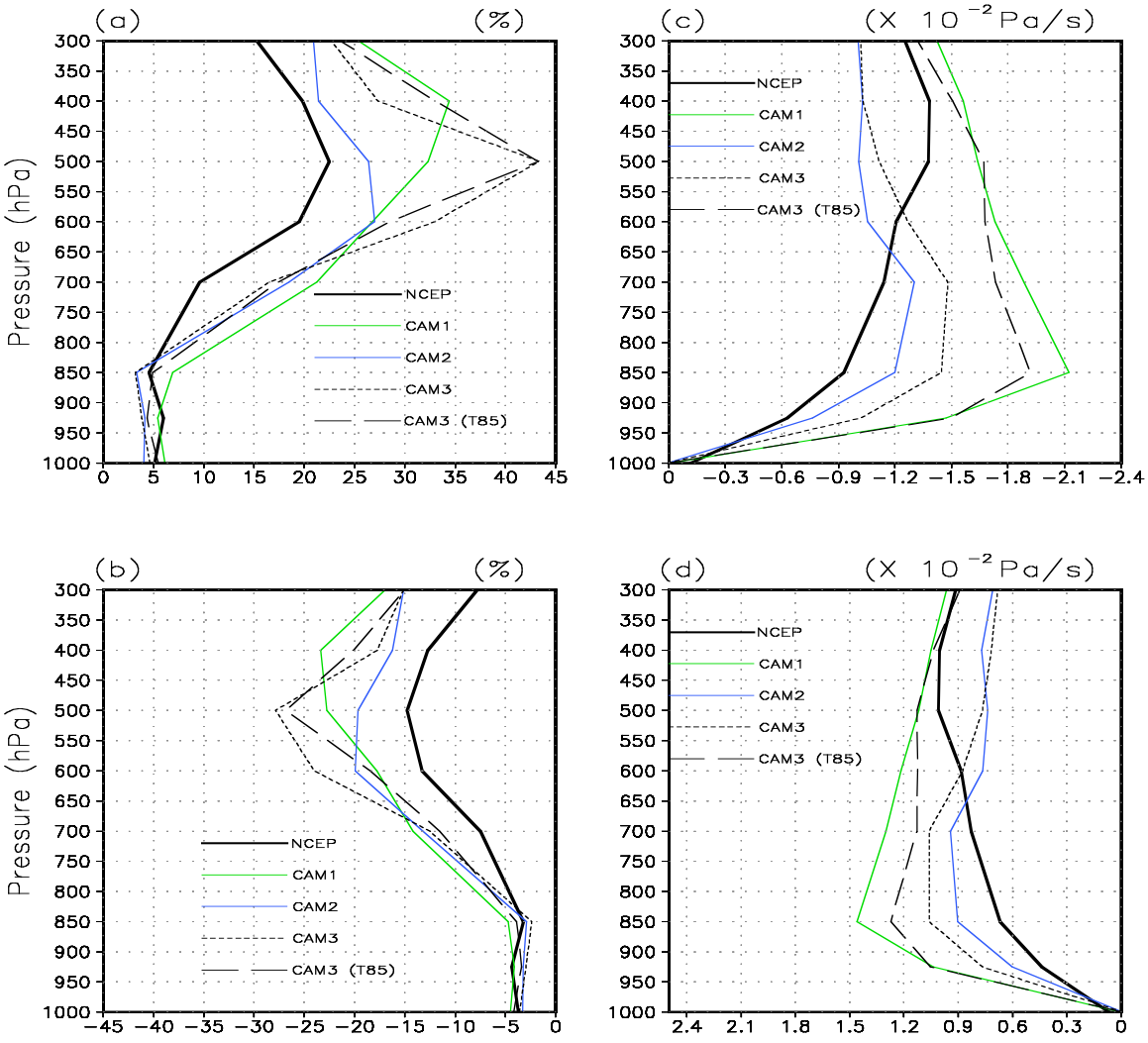

Figure 7: The composite percentage changes in specific humidity during (a) warm periods and (b) cold periods as a function of height from the NCEP-NCAR reanalysis and four models averaged over the equatorial Pacific (160°E-290°E, 5°S-5°N). The percentage changes in specific humidity are calculated as the anomalies divided by the respective climatology. Also shown are the composite changes in vertical velocity during (c) warm periods and (d) cold periods as a function of height from the NCEP-NCAR reanalysis and four models averaged over the equatorial Pacific (160°E-290°E, 5°S-5°N). The warm and cold periods are defined as the periods when the Niño-3 SST anomalies are larger than 0.3°C and less than -0.3°C over the ERBE period, respectively.

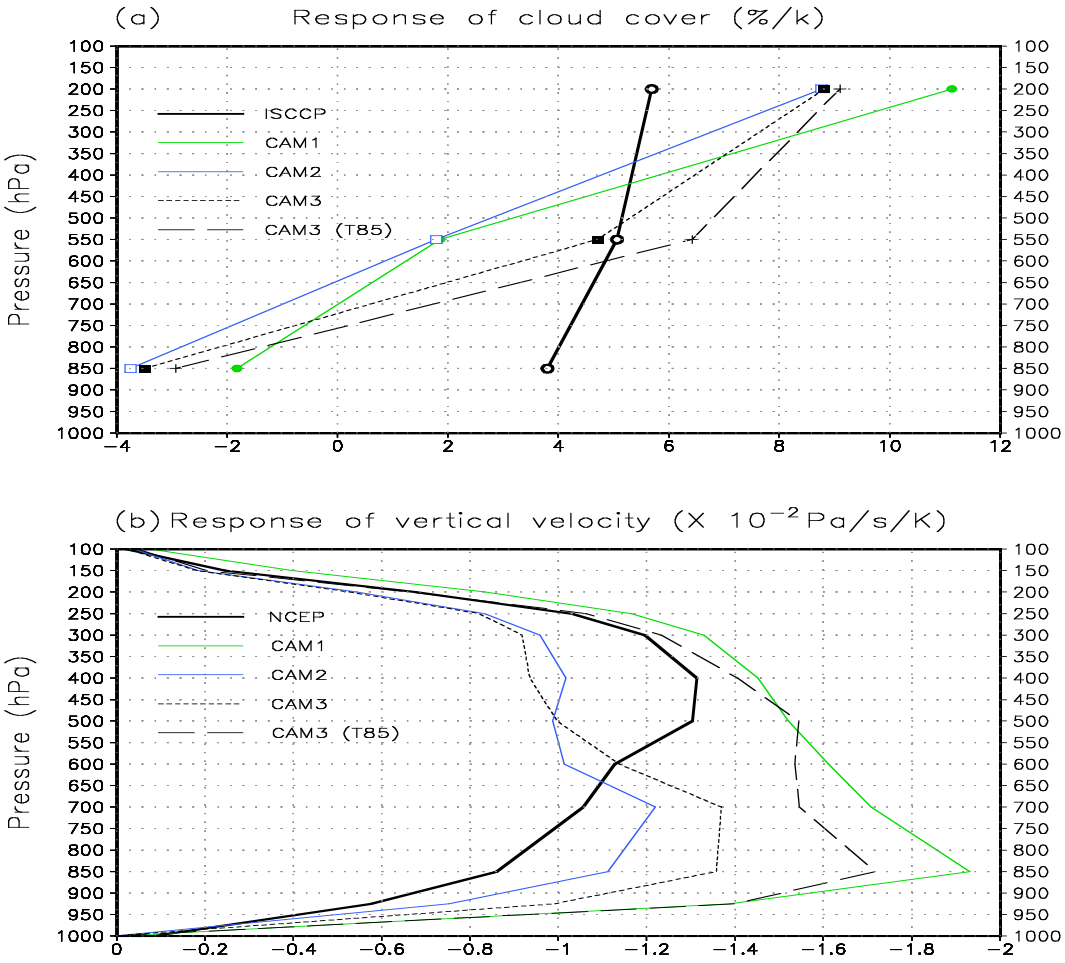

Figure 8: Responses of (a) cloud cover from ISCCP observations and four models, and (b) vertical velocity from the NCEP reanalysis and four models to El Niño warming as a function of height averaged over the equatorial Pacific (160°E-290°E, 5°S-5°N). The cloud cover data used here are the high, middle and low cloud cover (indicated by the markers shown in Fig.8a) for both models and observations, the same as those used by Sun et al. (2003) and Zhang and Sun (2006). Shown in every vertical level are regression coefficients obtained by linearly regressing the concerned quantities at the corresponding level against the underlying SST averaged over the region of El Niño warming (160°E-290°E, 5°S-5°N). The interannual variations of the concerned quantities over the ERBE period are used for the regression calculations.